Journal Name

RSCPublishing

Germanium nanocrystals as luminescent probes for rapid, sensitive and label-free detection of Fe^{3+} ions

Cite this: DOI: 10.1039/xoxxoooooox

Darragh Carolan* and Hugh Doyle*

Received ooth January 2012,
Accepted ooth January 2012

DOI: 10.1039/xoxxoooooox

www.rsc.org/

Luminescent water-soluble germanium nanocrystals (Ge NCs) have been developed as a fluorescent sensing platform for the highly selective and sensitive detection of Fe^{3+} *via* quenching of their strong blue luminescence, without the need for analyte-specific labelling groups. The amine-terminated Ge NCs were separated into two discrete size fractions with average diameters of 3.9 ± 0.4 nm and 6.8 ± 1.8 nm using centrifugation. The smaller 3.9 nm NCs possessed a strong blue luminescence, with an average lifetime of 6.1 ns and a quantum yield (QY) of 21.5 %, which is strongly influenced by solution pH. In contrast, 6.8 nm NCs exhibited a green luminescence with a longer lifetime of 7.8 ns and lower QY (6.2 %) that is insensitive to pH. Sensitive detection of Fe^{3+} was successfully demonstrated, with a linear relationship between luminescence quenching and Fe^{3+} concentration observed from 0-800 μM, with a limit of detection of 0.83 μM. The Ge NCs show excellent selectivity toward Fe^{3+} ions, with no quenching of the fluorescence signal induced by the presence of Fe^{2+} ions, allowing for solution phase discrimination between ions of the same element with different formal charges. The luminescence quenching mechanism was confirmed by static and time-resolved photoluminescence spectroscopies, while the applicability for this assay for detection of Fe^{3+} in real water samples was successfully demonstrated.

Introduction

Semiconductor nanocrystals have attracted much attention based on their unique optical and electrical properties, allowing for application in a wide range of areas including solar cells, light emitting devices,[1, 2] phosphors[3] and field-effect transistors.[4] Their chemical stability and resistance to photobleaching have made them particularly attractive as fluorescent probes for bio-imaging and labelling, opening up new strategies for simple, sensitive, on-site analysis of specific targets.[5, 6] Luminescent nanocrystals for chemical or biological sensing must be chemically robust to withstand challenging sample conditions, show minimal perturbation to the system probed (*i.e.*, low or no toxicity) and produce intense but switchable responses to incident light, yielding a strong signal change upon analyte interaction.[7, 8] Because of their high quantum yields and size tuneable emission profiles, nanocrystals based on II-VI materials (CdSe, CdTe, HgTe) have become one of the most extensively optical sensing nanomaterials in the detection of nucleic acids, enzymes, proteins, metal ions, and other small molecules.[9]

However, their optimal photophysical features are usually observed in organic solvents, thus restricting their analytical potential. While methods to render these NCs water-soluble and biocompatible have been reported, these protocols are compromised by reducing their photoluminescence efficiency. More problematic is the heavy metal content of these materials, which is toxic even at relatively low concentrations,[10-14] and may limit their wide scale use, particularly in clinical applications where the high disposal costs for heavy metal containing waste must be considered.

These toxicological concerns have driven the development of heavy metal free alternatives including Group IV materials[15-19] (*e.g.* Si, C) and ternary I-III-VI alloys[20] (*e.g.* $CuIn_xGa_{(1-x)}Se_2$, CIGS). In recent years, Ge NCs have emerged as environmentally friendlier alternatives to II-VI and IV-VI semiconductor materials as they are nontoxic, biocompatible and electrochemically stable.[21-23] As a result, Ge NCs have been increasingly used in applications ranging from biological imaging[24] to field effect transistors[25] and hybrid photodetectors.[26]

All sensing applications rely on the ability to prepare luminescent NCs with high quantum yields and well characterised surface chemistries, as these factors define many of their photophysical properties and response to analytes. A number of different solution phase approaches for synthesis of functionalised, luminescent Ge NCs have been reported, including the metathesis reaction of $GeCl_4$ with Zintl salts[27, 28] and high temperature decomposition of organogermane precursors.[29, 30] Other methods include thermal co-reduction of amido based precursors,[31] aqueous phase reduction of GeO_2 powders by $NaBH_4$,[32] reduction of germanium halides[33-37] and other high temperature chemical reduction methods.[38-40]

Disadvantages associated with these methods include synthetically involved precursor synthesis,[41] long reaction

times,[42] high temperatures and pressures,[29] and extensive post synthetic purification procedures.[43] Many groups also employ post synthetic purification techniques such as high performance liquid chromatography (HPLC),[33] column chromatography,[35, 36] controlled etching,[44] size-selective precipitation using non-solvents,[34, 38, 40, 45-47] or a combination of the above[48, 49] to chemically purify and separate size monodisperse Ge NCs fractions. While chromatography and HPLC methods work well for size separation, the method is generally reported only for small samples, and the rate of production is slow compared to simple centrifugation methods.

Iron is a biologically important and versatile ion and is ubiquitous in living systems,[50] playing a vital role in oxygen uptake, oxygen metabolism and electron transfer in the body. The presence of Fe^{3+} in biological systems has to be efficiently monitored as both its deficiency and overloading can induce various biological disorders[51, 52]; hence there is on-going requirement for sensitive sensing strategies for detection of iron.[53] While analytical techniques such as capillary electrophoresis,[54] electrochemical methods,[55] atomic absorption spectrometry (AAS)[56] and inductively coupled plasma mass spectrometry (ICP-MS),[57] are available for the detection of metal ions, they possess limitations including complicated processing, expensive instruments and time-consuming, complicated operation.[58, 59] Photoluminescence based sensing methods[60, 61] allow for rapid testing and analysis, possess high sensitivity due to the low signal backgrounds and excellent signal/noise ratios inherent to this method, and are relatively simple and cost effective to carry out.

In this paper, we report the synthesis of water-soluble Ge NCs as a fluorescent sensing platform for the highly selective and sensitive detection of Fe^{3+} *via* quenching of their strong blue luminescence. The Ge NCs produced here are purified by a combination of column chromatography and centrifugation to produce highly emissive nanocrystals for the sensitive detection of Fe^{3+} ions, without the need for specific labelling groups. In addition, the Ge NCs show excellent selectivity toward Fe^{3+} ions, with no quenching of the fluorescence signal induced by the presence of Fe^{2+} ions, allowing for solution phase discrimination between ions of the same element with different formal charges. The luminescence quenching mechanism was confirmed by lifetime and absorbance spectroscopies, while the applicability for this assay for detection of Fe^{3+} in real water samples was investigated.

Results and Discussion

Fig. 1(a) shows a transmission electron microscope (TEM) image of amine-terminated Ge NCs prepared by the reduction of germanium tetrachloride ($GeCl_4$) by lithium aluminium hydride ($LiAlH_4$) in the presence of tetrahexadeylammonium bromide (THDAB); see the ESI for further details on the synthesis and purification. As can be seen from this image, the Ge NCs produced are relatively polydisperse, with average sizes ranging from 3-12 nm, and evidence of some shape anisotropy in the sample. Fitting the histogram to a lognormal model yielded a mean diameter of 6.4 nm, with a standard deviation of 2.0 nm. Following centrifugation, the supernatant was decanted and the resultant pellet re-dispersed in deionised (DI) water.

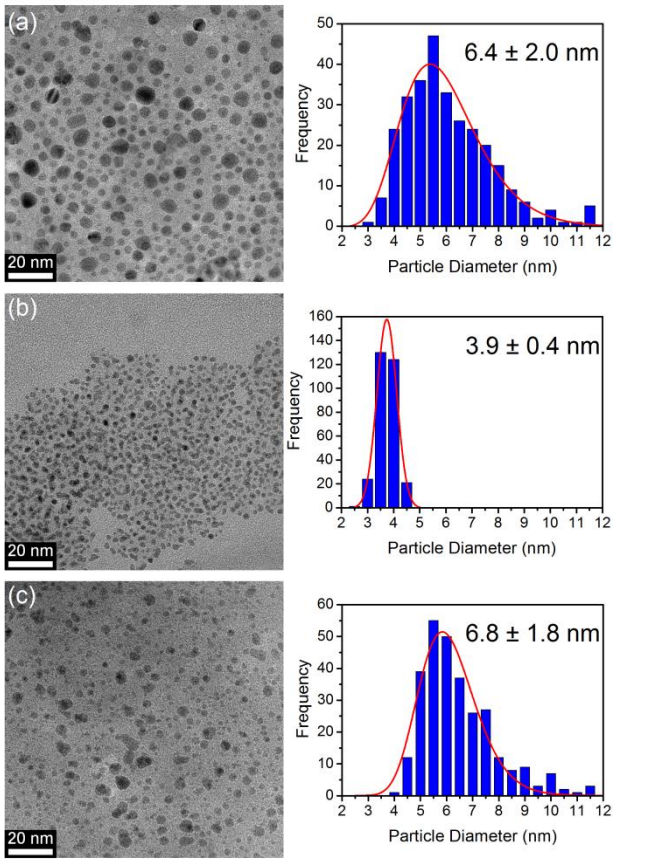

Fig. 1: Left, TEM images of the (a) parent solution, (b) supernatant and (c) pellet. Right, histograms of the NC size with curves fitted to the data using a lognormal model in the case of (a) and (c) and a Gaussian model in the case of (b).

TEM imaging of the supernatant, Fig. 1(b), demonstrates that it was possible to separate highly size and shape monodisperse NCs from the parent solution. The corresponding histogram was fitted with a Gaussian model, yielding a mean diameter of 3.9 nm and a standard deviation of 0.4 nm, closely matching the (111) spacing of bulk germanium, emphasizing the highly size monodisperse nature of these NCs. Fig. 1(c) shows a TEM image of the Ge NCs from pellet, with the corresponding histogram fitted with a lognormal model. It is evident that the size of the NCs is larger in the pellet, with an average diameter of 6.8 ± 1.8 nm. These TEM imaging results confirm that this simple centrifugation step results in the separation of a polydisperse parent solution into 2 fractions with differently sized NCs in each fraction. High resolution TEM (HR-TEM) imaging, (Fig. ESI1) shows that the Ge NCs are free of crystallographic defects with a lattice *d* spacing of 2.0 Å, matching well the (220) reflection of the Ge unit cell.

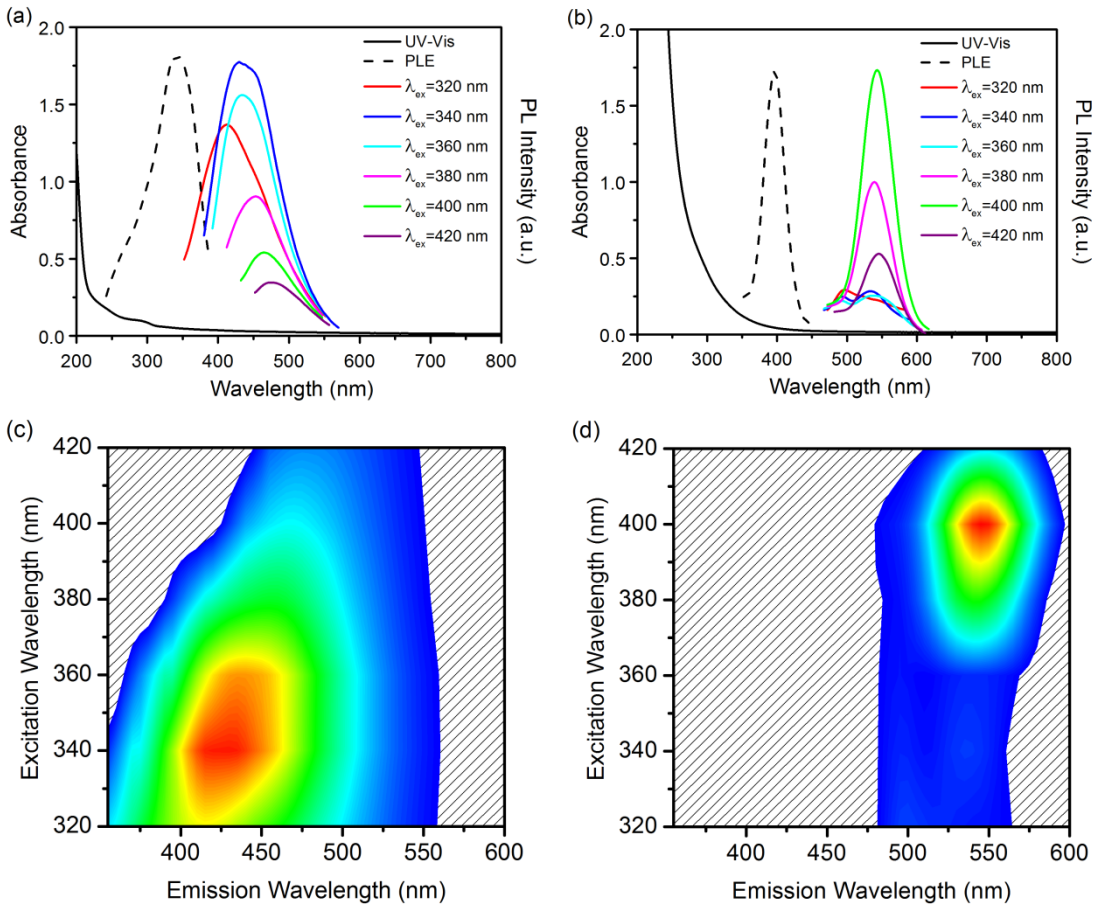

Fig. 2: UV-Vis, PL and PLE (dashed lines) spectra of (a) 3.9 nm and (b) 6.8 nm Ge NCs. Excitation-emission scanning matrices for (c) 3.9 nm and (d) 6.8 nm Ge NCs.

The optical properties of the Ge NCs were investigated using UV-Vis absorbance, photoluminescence (PL) and photoluminescence excitation (PLE) spectroscopy. Fig. 2(a) and (b) show the UV-Vis, PL and PLE spectra for the 3.9 nm and 6.8 nm NCs, respectively. The UV-Vis spectrum for the small NCs (Fig. 2(a)) shows weak absorption in the UV with a shoulder at *ca.* 290 nm and an onset of absorption at *ca.* 350 nm. These NCs show strong blue luminescence centred at *ca.* 430 nm, while the PLE spectrum (dashed line) recorded at the PL maximum shows a clear peak at 340 nm. The 6.8 nm NCs show a bathochromic shift in the onset of absorption and a stronger absorbance in the UV (see Fig. 2(b)), in agreement with our previous report on size tailored Ge NCs.[36] The larger NCs exhibited an intense green emission colour, with a wavelength maximum at *ca.* 540 nm, while the PLE spectrum showed a distinct peak at 400 nm. The PL spectra of both nanocrystal fractions demonstrated the strong excitation wavelength dependence, which we previously have shown to be due to the involvement of different surface states in the luminescence process rather than sample polydispersity.[37]

This excitation wavelength dependency for both NC fractions is shown graphically in the PL excitation-emission matrices presented in Fig. 2(c) and (d). For 3.9 nm Ge NCs, the strong blue luminescence observed shifts to longer wavelengths and decreases in intensity as the excitation wavelength is increased from 320 nm to 420 nm. In contrast, the intensity of the green photoluminescence increases with increasing excitation wavelength, without any significant shift in emission wavelength. The corresponding photoluminescence excitation-emission matrix for the parent solution shows the two emission bands visible at *ca.* 420 nm and *ca.* 540 nm, corresponding to the presence of both fractions, see Fig. ESI 2(a). The luminescence intensity of the PL spectra of the parent solution also reflects the individual excitation wavelength dependencies of both fractions, see Fig. ESI 2(b).

Fig. 3(a) shows the integrated PL intensity (340 nm excitation) of dilute dispersions of the 3.9 nm Ge NCs compared with solutions of the reference emitter 9,10-diphenylanthracene under identical excitation conditions.[62, 63] The quantum yield of the 3.9 nm NCs was calculated to be 21.5 %. Fig. 3(b) shows the integrated PL intensity (400 nm excitation) of dilute dispersions of the 6.8 nm Ge NCs compared with aqueous solutions of fluorescein, with a calculated quantum yield of 6.2 %. QY for both samples are in good comparison with the literature values. PL lifetimes of the Ge NCs were obtained using time-correlated single photon

counting methods; see Fig. 3(c). Measured transients were well fitted (χ^2 < 1.1) to the sum of two weighted exponentials, yielding an average lifetime of 6.1 ns for the 3.9 nm NCs and 7.8 ns for the 6.8 nm NCs, consistent with previous reports.[48, 64] The nanosecond lifetimes provide further confirmation that the Ge NCs luminescence arises from surface state recombination, as band gap transitions in indirect semiconductors typically occur on microsecond timescales.[65] The difference in PL lifetimes between the NC fractions is attributed to the involvement of different surface states in the luminescence process.

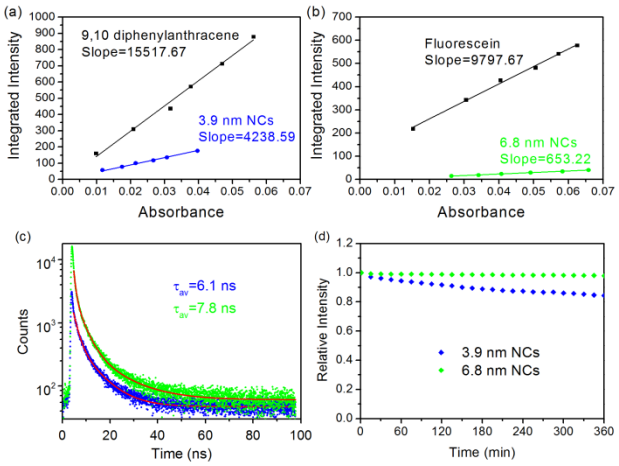

Fig. 3: Integrated PL intensity *vs.* absorbance for dilute dispersions of (a) 3.9 nm Ge NCs and 9,10-diphenylanthracene, (b) 6.8 nm Ge NCs and fluorescein. (c) PL decays of both NC samples and (d) long-term PL stability of both samples recorded over 6 hours.

The involvement of different surface species is demonstrated by PL measurements of the different Ge NC fractions taken under different pH conditions, see Fig. ESI 3. The 3.9 nm blue emitting NCs shows a strong response to the presence of H^+ ions, with a *ca.* 75 % decrease in PL intensity observed as the pH is lowered from 9.0 to 3.0. In contrast, the luminescence intensity of larger 6.8 nm NCs is insensitive to pH variations, implying that recombination does not involve surface species that are responsive to the presence of positive ions. As a result, luminescence quenching studies for the detection of metal ions in aqueous solution focused on the use of the brighter, more responsive 3.9 nm sized NCs. It is noted that both Ge NC fractions exhibit good to excellent long-term PL stability, decreasing by 15 % for the 3.9 nm NCs and only 2 % for the 6.8 nm NCs over a period of 6 hours, see Fig. 3(d).

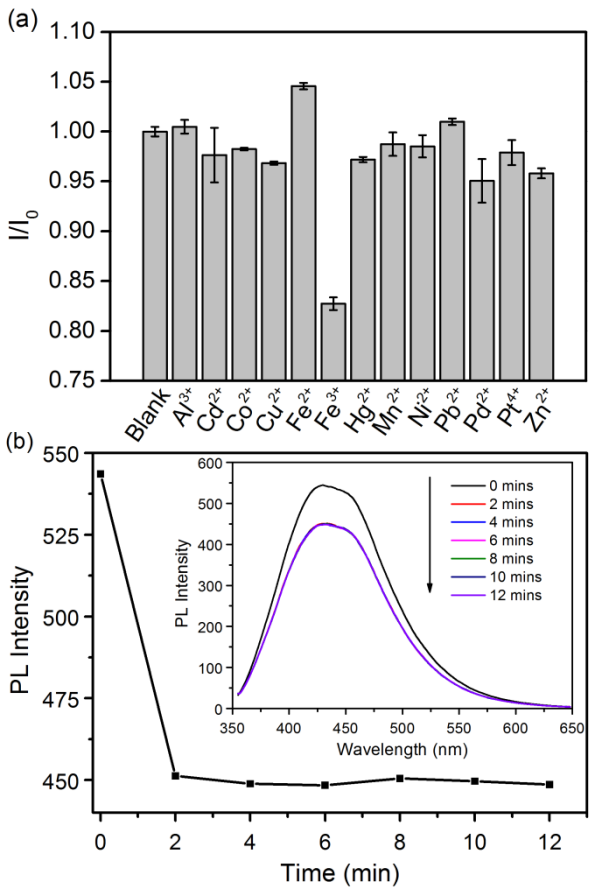

Fig. 4: (a) Normalised response for the effect of various different metal ions on the Ge NC fluorescence. (Concentration of ions is 50 µM). Error bars were calculated from the standard deviation of 6 measurements. (b) Time-dependent PL intensity obtained for the interaction between Ge NCs and Fe^{3+} ions. Inset shows the spectra obtained.

The luminescence quenching response of the blue emitting Ge NC to the presence of different metal ions (Al^{3+}, Cd^{2+}, Co^{2+}, Cu^{2+}, Fe^{2+}, Fe^{3+}, Hg^{2+}, Mn^{2+}, Ni^{2+}, Pb^{2+}, Pd^{2+}, Pt^{4+}, and Zn^{2+} ions), at a concentration of 50 µM in aqueous solution, is shown in Fig. 4(a). It was found that the Ge NCs exhibited a substantial (*ca.* 20 %) decrease in the PL intensity in the presence of Fe^{3+} ions, while only a modest response (typically less than 5% change) was observed for the other metal ions examined. More importantly, it is evident that the PL intensity of the Ge NCs in the presence of Fe^{2+} showed no decrease in intensity (in fact, a minor increase was observed), demonstrating that the nanocrystals can be used to selectively detect Fe^{3+} ions. Exposure tests carried out with Al^{3+} showed no evidence of a quenching response, demonstrating that the quenching response is selective towards iron, and not simply to the formal charge of the metal ions. Experiments carried out with Pt ions (formal charge: +4) also showed no change in PL intensity. This unusual selectivity demonstrated for a specific element and charge state make the Ge NCs a promising chemosensing platform for the highly efficient and sensitive detection of Fe^{3+}. The response time of this sensor was elucidated by monitoring the dependence of PL intensity on the

reaction time; see Fig. 4(b). The results showed that the PL intensity had reached a constant value within 2 minutes of addition of Fe^{3+}, indicating fast quenching kinetics; thereafter the PL intensity remains constant, see inset in Fig. 4(b).

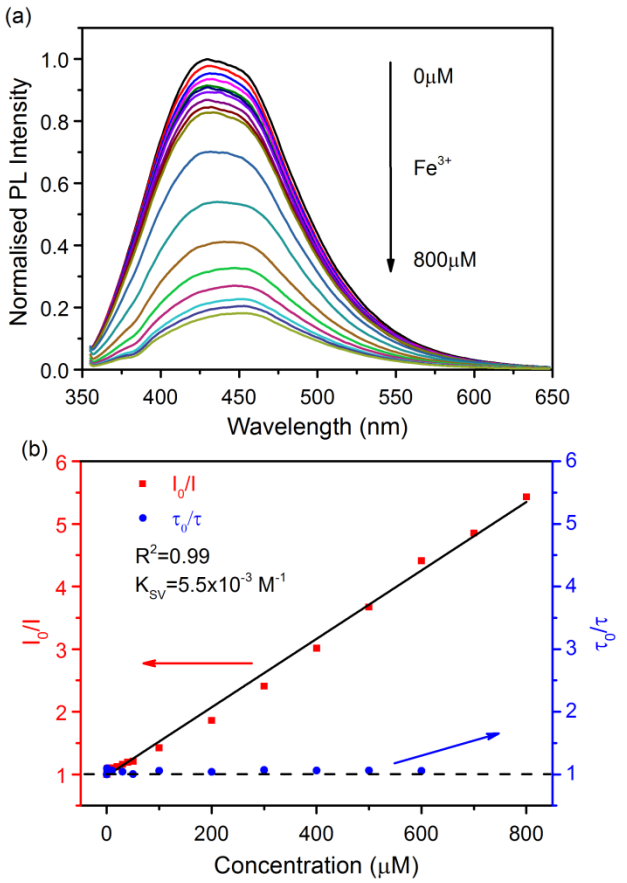

Fig. 5. (a) Representative photoluminescence spectra of Ge NCs in the presence of increasing Fe^{3+} concentrations (0-800 μM). (b) The relationship between I_0/I (red squares) and τ_0/τ (blue circles) with the concentration of Fe^{3+} ions within the range of 0-800 μM. The excitation was fixed at 340 nm for all spectra. I and I_0 are the PL intensities in the presence and absence of Fe^{3+} ions, respectively. τ and τ_0 are the lifetimes in the presence and absence of Fe^{3+} ions, respectively.

PL spectra were recorded at a series of different Fe^{3+} concentrations in order to evaluate the sensitivity of our Ge NCs sensing system for Fe^{3+} detection, see Fig. 5(a). Increasing the Fe^{3+} concentration from 0.25 μM to 800 μM resulted in a concomitant decrease in the PL intensity. The wavelength position of the emission maximum increased with increasing Fe^{3+} concentration, see Fig. ESI 4, indicating that a change in the surface states of the NCs has occurred.[66-69] Fig. 5(b) shows the dependence of I_0/I (red squares) on Fe^{3+} concentration, where I_0 and I are the PL intensities before and after addition of the analyte, respectively. The quenching data shows a linear relationship that is in excellent agreement with the Stern-Volmer relationship, $I_0/I=1+K_{SV}[Q]$, where K_{SV} is the Stern-Volmer constant and [Q] is the concentration of the quencher (Fe^{3+}). The lack of curvature in the plot indicates that only one quenching mechanism is present. Fitting the experimental data points with a least squares linear model over the range 0-800 μM yielded $K_{SV} = 5.5x10^{-3} \pm 0.1\ x10^{-3}\ M^{-1}$ with a correlation coefficient, $R^2 = 0.99$. The limit of detection (LOD) was determined to be 0.83 ± 0.02 μM, from the standard deviation of the blank (noise); LOD = $3\sigma_{blank}/K_{SV}$, according to the guidelines set by the International Union of Pure and Applied Chemistry (IUPAC).[70] A smaller LOD (54 ± 6 nM) could be obtained if the fitting was confined to the low concentration range (0.0-1.0 μM, however this resulted in a lower correlation coefficient ($R^2 = 0.98$) due to the fewer number of data points available for fitting, see Fig. ESI 5. To prove that the 3.9 nm NCs perform better than the 6.8 nm ones, the quenching efficiency (in the presence of 50 μM Fe^{3+}) of both sizes of NCs was compared, see Fig. ESI 6. Only a small response was observed for the 6.8 nm NCs, confirming the higher sensitivity of the small NCs.The mechanism for luminescence quenching is described as either a dynamic or static process: dynamic (or collisional) quenching occurs when the analyte (quencher) interacts with the excited state of the luminophore, resulting in a change in the lifetime of the excited state. The change in lifetime occurs because dynamic quenching is an additional rate process which depopulates the excited state, hence $I_0/I = \tau_0/\tau$, where τ_0 and τ are the excited state lifetimes in the absence and presence of the quencher, respectively. In contrast, static quenching results from the formation of a non-emissive ground state complex between the analyte and the nanocrystal: as the PL originates from non-complexed Ge NCs, the emissive lifetimes are unaffected.

PL lifetimes of the Ge NCs were measured over a range of Fe^{3+} concentrations, see blue symbols in Fig. 5(b). Increasing the Fe^{3+} concentration has no effect on the lifetime of the Ge NCs and τ_0/τ remains constant, consistent with the static quenching mechansim. Further confirmation of the static quenching mechanism was obtained from UV-Vis spectroscopy of the Ge NCs over a similar range of Fe^{3+} concentrations, see Fig. ESI 7. In the absence of Fe^{3+}, the Ge NCs absorb primarily in the UV region with a shoulder at *ca.* 290 nm and an onset of absorption at *ca.* 350 nm. Addition of Fe^{3+} ions to the NCs results in a red shift in the position of this shoulder to *ca.* 300 nm and the appearance of a second shoulder at *ca.* 260 nm is observed. While the spectrum of the Ge NCs in the presence of Fe^{3+} is largely different to its blank spectrum, the net spectrum[53] (Fe^{3+} alone subtracted from Ge NCs incubated with Fe^{3+}) is also different, see Fig. ESI 8. This indicates the conjugation of Fe^{3+} with the Ge NC surface.[60] These results provide further evidence that the Fe^{3+} induced PL quenching is due to formation of a non-emissive nanocrystal-analyte ground-state complex.

The ability of the Ge NCs to discriminate between Fe^{2+} and Fe^{3+} ions in solution may also be interpreted in terms of binding of ions to oxygenic species at the NC surface. Previous XPS measurements have shown the presence of significant amounts of oxygenic Ge-O_x species at the NC surface,[37] which are known to readily bind hard acids such as Al^{3+}, Cr^{3+} and Fe^{3+}. In contrast, softer acids such as Co^{2+}, Fe^{2+}, Ni^{2+}, Cu^{2+}, Zn^{2+} and Pb^{2+} show an affinity for nitrogen containing ligands. However, at the neutral pH used in these experiments, the amine ligands

(pK_a = 9.5-10.5) would be fully protonated, thus lessening their ability to bond to the positively charged ions. In contrast, the higher acidity of Ge-O_x species allows them to readily bind Fe^{3+} ions from solution, resulting in luminescence quenching. Furthermore, as no quenching response is elicited by the presence of 50 µM Al^{3+}, see Fig. 4(a), it may be inferred that the Ge NCs are selective toward iron, and not the +3 charge state.

Previous reports on Fe^{3+} detection have limitations including a narrow linear detection range,[71-78] lack of selectivity,[73-76, 78-80] and insufficient understanding of the quenching mechanism.[71, 75-77, 80-82] The excellent specificity, combined with high sensitivity and fast response time, suggested that the Ge NCs were applicable for detection Fe^{3+} in real water samples. The performance of the Ge NC sensing platform for Fe^{3+}detection was tested on samples obtained from drinkable (tap) water supplies, and fresh water samples from local rivers and lakes, see Fig. ESI 9. Despite the presence of minerals, organic matter and other contaminants, the Ge NCs exhibited a linear relationship between PL intensity and Fe^{3+} concentration (1-200 µM range) for all the real water samples, satisfying the US Environmental Protection Agency requirements (0.3 mg/L; ≈ 5.4 µM) for Fe^{3+} levels in drinkable water supplies.[83] Table ESI 1 shows that the recovery of Fe^{3+} was between 97-110 % for the real water samples, demonstrating the applicability and robustness of this detection procedure.

Conclusions

The synthesis of highly luminescent, water-soluble Ge NCs for the sensitive detection of Fe^{3+} ions, without the need for specific labelling groups has been reported. The amine-terminated Ge NCs were separated into two discrete size fractions with average diameters of 3.9 ± 0.4 nm and 6.8 ± 1.8 nm using centrifugation. The smaller 3.9 nm NCs possessed a strong blue luminescence, with an average lifetime of 6.1 ns and a QY of 21.5 %, which is strongly influenced by solution pH. In contrast, 6.8 nm NCs exhibited a green luminescence with a longer lifetime of 7.8 ns and lower QY (6.2 %) that is insensitive to pH. Sensitive detection of Fe^{3+} was successfully demonstrated, with a linear relationship between luminescence quenching and Fe^{3+} concentration observed from 0-800 µM, with a limit of detection of 0.83 µM. The luminescence quenching mechanism was confirmed to be a static quenching mechanism, while the applicability for this assay for detection of Fe^{3+} in real water samples was successfully demonstrated.

Acknowledgements

This work was supported by the European Commission under the FP7 Projects HYSENS (grant agreement n° 263091), COMMONSENSE (grant agreement n° 261809) and SNAPSUN (grant agreement n° 246310), as well as the Irish Higher Education Authority under the PRTLI programs (Cycle 3 "Nanoscience" and Cycle 4 "INSPIRE"

Notes and references

Tyndall National Institute, University College Cork, Lee Maltings, Cork, Ireland.

**Email: darragh.carolan@tyndall.ie; hugh.doyle@tyndall.ie.*

Electronic Supplementary Information (ESI) available: Experimental methods, optical properties of the parent sample, pH dependence of the NC fractions, Stern-Volmer plot for the concentration range 0-1 µM, spectra and Stern-Volmer plots for the NCs in various real water samples.]. See DOI: 10.1039/b000000x/

1. Y. Shirasaki, G. J. Supran, M. G. Bawendi and V. Bulovic, *Nat. Photonics*, 2013, **7**, 13.
2. V. Wood and V. Bulović, *Nano Reviews*, 2010, **1**, 5202.
3. E. Mutlugun, P. L. Hernandez-Martinez, C. Eroglu, Y. Coskun, T. Erdem, V. K. Sharma, E. Unal, S. K. Panda, S. G. Hickey, N. Gaponik, A. Eychmüller and H. V. Demir, *Nano Lett.*, 2012, **12**, 3986.
4. D. V. Talapin, J.-S. Lee, M. V. Kovalenko and E. V. Shevchenko, *Chem. Rev.*, 2009, **110**, 389.
5. C. M. Tyrakowski and P. T. Snee, *Phys. Chem. Chem. Phys.*, 2014, **16**, 837.
6. X. Michalet, F. F. Pinaud, L. A. Bentolila, J. M. Tsay, S. Doose, J. J. Li, G. Sundaresan, A. M. Wu, S. S. Gambhir and S. Weiss, *Science*, 2005, **307**, 538.
7. A. E. Nel, L. Madler, D. Velegol, T. Xia, E. M. V. Hoek, P. Somasundaran, F. Klaessig, V. Castranova and M. Thompson, *Nat. Mater*, 2009, **8**, 543.
8. J. E. Gagner, S. Shrivastava, X. Qian, J. S. Dordick and R. W. Siegel, *J. Phys. Chem. Lett.*, 2012, **3**, 3149.
9. P. D. Howes, R. Chandrawati and M. M. Stevens, *Science*, 2014, **346**, 1247390.
10. M. Bottrill and M. Green, *Chem. Commun.*, 2011, **47**, 7039.
11. E. P. a. o. t. Council, Directive 2002/95/EC on the restriction of the use of certain hazardous substances in electrical and electronic equipment, www.eur-lex.europa.eu.
12. L. Ye, K.-T. Yong, L. Liu, I. Roy, R. Hu, J. Zhu, H. Cai, W.-C. Law, J. Liu, K. Wang, J. Liu, Y. Liu, Y. Hu, X. Zhang, M. T. Swihart and P. N. Prasad, *Nat. Nanotechnol.*, 2012, **7**, 453.
13. F. M. Winnik and D. Maysinger, *Acc. Chem. Res.*, 2012, **46**, 672.
14. A. M. Derfus, W. C. W. Chan and S. N. Bhatia, *Nano Lett.*, 2003, **4**, 11.
15. N. Shirahata, *Phys. Chem. Chem. Phys.*, 2011, **13**, 7284.
16. K. Dohnalová, T. Gregorkiewicz and K. Kůsová, *J. Phys.: Condens. Matter*, 2014, **26**, 173201.
17. S. N. Baker and G. A. Baker, *Angew. Chem. Int. Ed.*, 2010, **49**, 6726.
18. H. Li, Z. Kang, Y. Liu and S.-T. Lee, *J. Mater. Chem.*, 2012, **22**, 24230.
19. J. C. G. Esteves da Silva and H. M. R. Gonçalves, *TrAC, Trends Anal. Chem.*, 2011, **30**, 1327.
20. H. Zhong, Z. Bai and B. Zou, *J. Phys. Chem. Lett.*, 2012, **3**, 3167.
21. S. Bhattacharjee, I. M. C. M. Rietjens, M. P. Singh, T. M. Atkins, T. K. Purkait, Z. Xu, S. Regli, A. Shukaliak, R. J. Clark, B. S. Mitchell, G. M. Alink, A. T. M. Marcelis, M. J. Fink, J. G. C. Veinot, S. M. Kauzlarich and H. Zuilhof, *Nanoscale*, 2013, **5**, 4870.
22. D. D. Vaughn II and R. E. Schaak, *Chem. Soc. Rev.*, 2013, **42**, 2861.
23. R. Pillarisetty, *Nature*, 2011, **479**, 324.
24. T. N. Lambert, N. L. Andrews, H. Gerung, T. J. Boyle, J. M. Oliver, B. S. Wilson and S. M. Han, *Small*, 2007, **3**, 691.
25. Z. C. Holman, C.-Y. Liu and U. R. Kortshagen, *Nano Lett.*, 2010, **10**, 2661.
26. D.-J. Xue, J.-J. Wang, Y.-Q. Wang, S. Xin, Y.-G. Guo and L.-J. Wan, *Adv. Mater.*, 2011, **23**, 3704.
27. B. R. Taylor, S. M. Kauzlarich, G. R. Delgado and H. W. H. Lee, *Chem. Mater.*, 1999, **11**, 2493.
28. A. J. Pugsley, C. L. Bull, A. Sella, G. Sankar and P. F. McMillan, *J. Solid. State. Chem.*, 2011, **184**, 2345.

29. N. Zaitseva, Z. R. Dai, C. D. Grant, J. Harper and C. Saw, *Chem. Mater.*, 2007, **19**, 5174.
30. X. M. Lu, K. J. Ziegler, A. Ghezelbash, K. P. Johnston and B. A. Korgel, *Nano Lett.*, 2004, **4**, 969.
31. H. Gerung, S. D. Bunge, T. J. Boyle, C. J. Brinker and S. M. Han, *Chem. Commun.*, 2005, 1914.
32. J. Wu, Y. Sun, R. Zou, G. Song, Z. Chen, C. Wang and J. Hu, *CrystEngComm*, 2011, **13**, 3674.
33. J. P. Wilcoxon, P. P. Provencio and G. A. Samara, *Phys. Rev. B*, 2001, **64**, 035417.
34. E. Fok, M. L. Shih, A. Meldrum and J. G. C. Veinot, *Chem. Commun.*, 2004, 386.
35. S. Prabakar, A. Shiohara, S. Hanada, K. Fujioka, K. Yamamoto and R. D. Tilley, *Chem. Mater.*, 2010, **22**, 482.
36. D. Carolan and H. Doyle, *J. Mater. Chem. C*, 2014, **2**, 3562.
37. D. Carolan and H. Doyle, *J. Nanopart. Res.*, 2014, **16**, 1.
38. S. C. Codoluto, W. J. Baumgardner and T. Hanrath, *CrystEngComm*, 2010, **12**, 2903.
39. W. Z. Wang, B. Poudel, J. Y. Huang, D. Z. Wang, S. Kunwar and Z. F. Ren, *Nanotechnology*, 2005, **16**, 1126.
40. D. A. Ruddy, J. C. Johnson, E. R. Smith and N. R. Neale, *ACS Nano*, 2010, **4**, 7459.
41. B. R. Taylor, S. M. Kauzlarich, H. W. H. Lee and G. R. Delgado, *Chem. Mater.*, 1998, **10**, 22.
42. X. Ma, F. Wu and S. M. Kauzlarich, *J. Solid. State. Chem.*, 2008, **181**, 1628.
43. E. Muthuswamy, A. S. Iskandar, M. M. Amador and S. M. Kauzlarich, *Chem. Mater.*, 2012, **25**, 1416.
44. S. Kim, B. Walker, S. Y. Park, H. Choi, S.-J. Ko, J. Jeong, M. H. Yun, J. C. Lee, D. S. Kim and J. Y. Kim, *Nanoscale*, 2014, **6**, 10156.
45. D. D. Vaughn, II, J. F. Bondi and R. E. Schaak, *Chem. Mater.*, 2010, **22**, 6103.
46. X. M. Lu, B. A. Korgel and K. P. Johnston, *Chem. Mater.*, 2005, **17**, 6479.
47. D. C. Lee, J. M. Pietryga, I. Robel, D. J. Werder, R. D. Schaller and V. I. Klimov, *J. Am. Chem. Soc.*, 2009, **131**, 3436.
48. N. Shirahata, D. Hirakawa, Y. Masuda and Y. Sakka, *Langmuir*, 2012, **29**, 7401.
49. N. Shirahata, *J. Solid. State. Chem.*, 2014, **214**, 74.
50. F. A. Cotton and G. Wilkinson, *Advanced Inorganic Chemistry*, Wiley, New York, 1989.
51. N. C. Andrews, *N. Engl. J. Med.*, 1999, **341**, 1986.
52. D. Galaris, V. Skiada and A. Barbouti, *Cancer Lett.*, 2008, **266**, 21.
53. J. Zhang, Y. Yuan, Z.-L. Yu, A. Yu and S.-H. Yu, *Small*, 2014, **10**, 3662.
54. I. Ali and H. Y. Aboul-Enein, *Anal. Lett.*, 2002, **35**, 2053.
55. G. Aragay and A. Merkoçi, *Electrochim. Acta*, 2012, **84**, 49.
56. J. V. Cizdziel and S. Gerstenberger, *Talanta*, 2004, **64**, 918.
57. A. T. Townsend, K. A. Miller, S. McLean and S. Aldous, *J. Anal. At. Spectrom.*, 1998, **13**, 1213.
58. M. Leermakers, W. Baeyens, P. Quevauviller and M. Horvat, *TrAC, Trends Anal. Chem.*, 2005, **24**, 383.
59. Y. Li, C. Chen, B. Li, J. Sun, J. Wang, Y. Gao, Y. Zhao and Z. Chai, *J. Anal. At. Spectrom.*, 2006, **21**, 94.
60. J. Zhang and S.-H. Yu, *Nanoscale*, 2014, **6**, 4096.
61. P. Yang, Y. Zhao, Y. Lu, Q.-Z. Xu, X.-W. Xu, L. Dong and S.-H. Yu, *ACS Nano*, 2011, **5**, 2147.
62. A. T. R. Williams, S. A. Winfield and J. N. Miller, *Analyst*, 1983, **108**, 1067.
63. J. R. Lakowicz, *Principles of fluorescence spectroscopy*, Springer-Verlag, New York, 2008.
64. J. H. Warner and R. D. Tilley, *Nanotechnology*, 2006, **17**, 3745.
65. M. Dasog, Z. Yang, S. Regli, T. M. Atkins, A. Faramus, M. P. Singh, E. Muthuswamy, S. M. Kauzlarich, R. D. Tilley and J. G. C. Veinot, *ACS Nano*, 2013, **7**, 2676.
66. A. V. Isarov and J. Chrysochoos, *Langmuir*, 1997, **13**, 3142.
67. Y.-S. Xia, C. Cao and C.-Q. Zhu, *JOL*, 2008, **128**, 166.
68. C. Dong, H. Qian, N. Fang and J. Ren, *J. Phys. Chem. B*, 2006, **110**, 11069.
69. A. Eychmüller, A. Hässelbarth and H. Weller, *JOL*, 1992, **53**, 113.
70. C. Analytical Methods, *Analyst*, 1987, **112**, 199.
71. T. Lai, E. Zheng, L. Chen, X. Wang, L. Kong, C. You, Y. Ruan and X. Weng, *Nanoscale*, 2013, **5**, 8015.
72. Y.-L. Zhang, L. Wang, H.-C. Zhang, Y. Liu, H.-Y. Wang, Z.-H. Kang and S.-T. Lee, *RSC Adv.*, 2013, **3**, 3733.
73. K. Qu, J. Wang, J. Ren and X. Qu, *Chem. Eur. J.*, 2013, **19**, 7243.
74. L. Zhu, Y. Yin, C.-F. Wang and S. Chen, *J. Mater. Chem. C*, 2013, **1**, 4925.
75. J. Xu, Y. Zhou, S. Liu, M. Dong and C. Huang, *Anal. Methods*, 2014, **6**, 2086.
76. W. Li, Z. Zhang, B. Kong, S. Feng, J. Wang, L. Wang, J. Yang, F. Zhang, P. Wu and D. Zhao, *Angew. Chem. Int. Ed.*, 2013, **52**, 8151.
77. J. Xu, T. Lai, Z. Feng, X. Weng and C. Huang, *Luminescence*, 2014, n/a.
78. A. Zhao, C. Zhao, M. Li, J. Ren and X. Qu, *Anal. Chim. Acta*, 2014, **809**, 128.
79. L. Q. Liu, Y. F. Li, L. Zhan, Y. Liu and C. Z. Huang, *Sci. China-Chem.*, 2011, **54**, 1342.
80. S. Zhu, Q. Meng, L. Wang, J. Zhang, Y. Song, H. Jin, K. Zhang, H. Sun, H. Wang and B. Yang, *Angew. Chem. Int. Ed.*, 2013, **52**, 3953.
81. S. Qu, H. Chen, X. Zheng, J. Cao and X. Liu, *Nanoscale*, 2013, **5**, 5514.
82. H. Ding, J.-S. Wei and H.-M. Xiong, *Nanoscale*, 2014, **6**, 13817.
83. U. S. E. P. A., *Code of Federal Regulations Part 143-National Secondary Drinking Water Regulations*, 2009.